Available online at www.sciencedirect.com

SciVerse ScienceDirect

Advances in Space Research 51 (2013) 1916–1923

ADVANCES IN SPACE RESEARCH (a COSPAR publication)

www.elsevier.com/locate/asr

Magnetohydrodynamics in solar and space physics

Daniel Gómez [a,b,*], Luis N. Martín [b], Pablo Dmitruk [b]

[a] Instituto de Astronomía y Física del Espacio, Casilla de Correo 67, Sucursal 28, 1428 Buenos Aires, Argentina
[b] Departamento de Física, Facultad de Ciencias Exactas y Naturales, Universidad de Buenos Aires, Pabellón I – Ciudad Universitaria, 1428 Buenos Aires, Argentina

Available online 24 September 2012

Abstract

Because of its proximity, our Sun provides a unique opportunity to perform high resolution observations of its outer layers throughout the whole electromagnetic spectrum. We can also theoretically model most of the fascinating physical phenomena taking place on the Sun, as well as their impact on the solar system.

Many of these phenomena can be properly studied within the framework of magnetohydrodynamics. More specifically, we assume a fully ionized hydrogen plasma and adopt the more comprehensive two-fluid magnetohydrodynamic approximation. For problems such as the solar wind or magnetic loops in the solar corona, which are shaped by a relatively strong mean magnetic field, the reduced magnetohydrodynamic approximation is often used.

We will review the basic features of both two-fluid and one-fluid magnetohydrodynamics, and focus on two particular applications: the turbulent heating of coronal active regions and the dynamics of the solar wind.
© 2012 COSPAR. Published by Elsevier Ltd. All rights reserved.

Keywords: Magnetohydrodynamics; Turbulence; Solar physics; Space physics

1. Introduction

Magnetohydrodynamics (MHD) is a reasonable theoretical framework to describe the large-scale dynamics of a plasma, which is also known as one-fluid MHD. Two-fluid effects can be considered through a generalized Ohm's law which includes the Hall current, which is required for phenomena with characteristic length scales comparable or smaller than the ion skin depth c/ω_{pi} (c:speed of light, ω_{pi}: ion plasma frequency). In an ideal plasma, the Hall current causes the magnetic field to become frozen in the electron flow instead of being carried along with the bulk velocity field. Another relevant feature of the ideal Hall MHD description is the self-consistent presence of parallel (to the magnetic field) electric fields, which can therefore accelerate particles.

In astrophysical plasmas, a strong external magnetic field is often present, thus breaking down the isotropy of the problem and eventually causing important changes in the dynamics of these plasmas. For one-fluid MHD, the presence of an external magnetic field gave rise to the so-called reduced MHD approximation (RMHD, see Strauss (1976); Montgomery (1982)). The RMHD equations have been used in a variety of astrophysical applications, such as current sheet formation (van Ballegooijen, 1986; Longcope and Sudan, 1994), non-stationary reconnection (Hendrix and van Hoven, 1996; Milano et al., 1999), the dynamics of coronal loops (Gómez and Ferro Fontán, 1992; Dmitruk and Gómez, 1999) or the development of turbulence (Dmitruk et al., 2003). Dmitruk et al. (2005) have numerically confirmed the validity of the RMHD equations by directly comparing its predictions with the compressible MHD equations in a turbulent regime. More recently, Gómez et al. (2008) extended the "reduced" approximation to include two-fluid effects, giving rise to

* Corresponding author at: Departamento de Física, Facultad de Ciencias Exactas y Naturales, Universidad de Buenos Aires, Pabellón I – Ciudad Universitaria, 1428 Buenos Aires, Argentina. Tel.: +54 11 47890179; fax: +54 11 47868114.

E-mail addresses: gomez@iafe.uba.ar (D. Gómez), lmartin@df.uba.ar (L.N. Martín), pdmitruk@df.uba.ar (P. Dmitruk).

0273-1177/$36.00 © 2012 COSPAR. Published by Elsevier Ltd. All rights reserved.
http://dx.doi.org/10.1016/j.asr.2012.09.016

the reduced Hall-MHD description (RHMHD, see also Bian and Tsiklauri (2009)). A comparative study of numerical simulations of the compressible three-dimensional Hall-MHD equations and the reduced approximation, has recently confirmed the validity of the RHMHD description in the asymptotic limit of strong external magnetic fields (Martín et al., 2010).

We organize the paper as follows. After introducing the Hall-MHD set of equations in Section 2, we perform the asymptotic expansion corresponding to the dynamics of a plasma embedded in a strong external magnetic field in Section 3, and derive the set of RHMHD equations. In Section 4 we integrate the RHMHD to simulate the development of turbulence in the solar wind. More specifically, we show that the presence of the Hall effect causes non-negligible changes in the energy power spectrum and also discuss the consequences of an electric field component which is parallel to the magnetic field. We also applied the one-fluid version of these equations (i.e. the RMHD equations) to simulate the internal dynamics of loops of the solar corona. The main results from these simulations are summarized in Section 5, showing the development of a turbulent regime in these loops, which enhances Joule dissipation to levels consistent with the energy requirements to heat active regions. Finally, in Section 6 we summarize our conclusions.

2. The Hall-MHD equations

The large-scale dynamics of a multispecies plasma can be described through fluid equations for each species s (see for instance Goldston and Rutherford (1995))

$$\partial_t n_s + \nabla\cdot(n_s \boldsymbol{U}_s) = 0 \tag{1}$$

$$m_s n_s \frac{d\boldsymbol{U}_s}{dt} = n_s q_s\left(\boldsymbol{E} + \frac{1}{c}\boldsymbol{U}_s\times\boldsymbol{B}\right) - \nabla p_s + \nabla\cdot\sigma_s + \sum_{s'} R_{ss'} \tag{2}$$

where m_s, q_s are the individual mass and charge of particles of species s, n_s, $\boldsymbol{U}_s$, p_s are their particle density, velocity field and scalar pressure respectively, while σ_s is the viscous stress tensor and $R_{ss'}$ is the rate of momentum (per unit volume) gained by species s due to collisions with species s'. In the presence of a strong magnetic field, pressure might depart from scalar and become anisotropic (i.e. $p_\parallel \neq p_\perp$), but we are neglecting this effect throughout this paper. The momentum exchange $R_{ss'}$ rate is proportional to the relative speed between both species and is given by

$$R_{ss'} = -m_s n_s \nu_{ss'}(\boldsymbol{U}_s - \boldsymbol{U}_{s'}) \tag{3}$$

where $\nu_{ss'}$ is the collision frequency of an s-particle against particles of species s'. Since the total momentum must of course be conserved, the corresponding exchange rates satisfy $R_{s's} = -R_{ss'}$, from which it follows that collision frequencies must obey $m_s n_s \nu_{ss'} = m_{s'} n_{s'} \nu_{s's}$. The electric current density for a multi-species plasma is defined as

$$\boldsymbol{J} = \sum_s q_s n_s \boldsymbol{U}_s \tag{4}$$

The equations of motion for a fully ionized hydrogen plasma, made of protons of particle mass m_p and electrons of negligible mass (since $m_e \ll m_p$) are given by Krall and Trivelpiece (1973)

$$m_p n \frac{d\boldsymbol{U}}{dt} = en\left(\boldsymbol{E} + \frac{1}{c}\boldsymbol{U}\times\boldsymbol{B}\right) - \nabla p_p + \nabla\cdot\sigma + R \tag{5}$$

$$0 = -en\left(\boldsymbol{E} + \frac{1}{c}\boldsymbol{U}_e\times\boldsymbol{B}\right) - \nabla p_e - R \tag{6}$$

where $\boldsymbol{U}$, $\boldsymbol{U}_e$ are the ion and electron flow velocities. The viscous stress tensor for electrons has been neglected, since it is proportional to the particle mass, and the friction force between both species can be written as

$$R = -m_p n \nu_{pe}(\boldsymbol{U} - \boldsymbol{U}_e) \tag{7}$$

For the fully ionized hydrogen case, the electric current density (see Eq. (4)) reduces to $\boldsymbol{J} = en(\boldsymbol{U} - \boldsymbol{U}_e)$. Therefore, the friction force R can be expressed as

$$R = -\frac{m_p \nu_{pe}}{e}\boldsymbol{J} \tag{8}$$

The electron and ion pressures p_e, p_p are assumed to satisfy polytropic laws

$$p_p \propto n^\gamma \tag{9}$$

$$p_e \propto n^\gamma \tag{10}$$

where the particle densities for both species are assumed to be equal because of charge neutrality (i.e. $n_p = n_e = n$). The bulk flow in this two-fluid description is given by the ion flow $\boldsymbol{U}$, which satisfies

$$\partial_t n + \nabla\cdot(n\boldsymbol{U}) = 0 \tag{11}$$

The electric current density relates with the magnetic field through Ampere's law

$$\boldsymbol{J} = \frac{c}{4\pi}\nabla\times\boldsymbol{B} = en(\boldsymbol{U} - \boldsymbol{U}_e) \tag{12}$$

By adding Eqs. (5) and (6) and adopting a Newtonian prescription for the viscous stress tensor (i.e. $\sigma_{ij} = \mu(\partial_i U_j + \partial_j U_i)$, μ: viscosity) we obtain

$$m_p n \frac{d\boldsymbol{U}}{dt} = \frac{1}{c}\boldsymbol{J}\times\boldsymbol{B} - \nabla p + \mu\nabla^2\boldsymbol{U} \tag{13}$$

where $p = p_p + p_e$. On the other hand, after replacing $\boldsymbol{U}_e = \boldsymbol{U} - \boldsymbol{J}/en$ and Eq. (8) into Eq. (6), we obtain the so-called "generalized Ohm's law"

$$\boldsymbol{E} + \frac{1}{c}\boldsymbol{U}\times\boldsymbol{B} = \frac{1}{nec}\boldsymbol{J}\times\boldsymbol{B} - \frac{1}{ne}\nabla p_e + \frac{m_p\nu_{pe}}{e^2 n}\boldsymbol{J} \tag{14}$$

which also expresses the force balance satisfied by the massless electrons. In the last term, we can recognize $e^2 n/(m_p\nu_{pe})$ as the electric conductivity of a fully ionized hydrogen plasma. The electric and magnetic fields can be cast in terms of the electrostatic potential ϕ and the vector potential $\boldsymbol{A}$. In particular, the curl of Eq. (14) yields the induction equation

$$\partial_t\boldsymbol{B} = \nabla\times\left[\left(\boldsymbol{U} - \frac{1}{en}\boldsymbol{J}\right)\times\boldsymbol{B}\right] - \nabla\times(\eta\nabla\times\boldsymbol{B}) \tag{15}$$

where

$$\eta = \frac{mc^2 \nu_{pe}}{4\pi e^2 n} \tag{16}$$

is the electric resistivity. Eqs. (13)–(15) provide the two-fluid description of magnetohydrodynamics. The set of equations is completed by the continuity equation (Eq. (11)), the adiabatic conditions given by Eqs. (9), (10) and Ampere's law (Eq. (12)).

We now turn to a dimensionless version of the preceding set of equations using a typical longitudinal length scale L_0, an ambient density $n = n_0$, a typical value for the magnetic field B_0, a typical velocity equal to the Alfven speed $v_A = B_0/\sqrt{4\pi m_p n_0}$, and a reference pressure p_0. The equation of motion becomes

$$n\frac{d\boldsymbol{U}}{dt} = (\nabla \times \boldsymbol{B}) \times \boldsymbol{B} - \beta \nabla p + \frac{1}{Re}\nabla^2 \boldsymbol{U} \tag{17}$$

while the induction equation can be written as

$$\partial_t \boldsymbol{B} = \nabla \times \left[\left(\boldsymbol{U} - \frac{\epsilon}{n}\nabla \times \boldsymbol{B}\right) \times \boldsymbol{B}\right] + \frac{1}{Rm}\nabla^2 \boldsymbol{B} \tag{18}$$

The various dimensionless coefficients in these equations measure the relative importance of different competing physical effects. The plasma "*beta*"

$$\beta = \frac{p_0}{m_p n_0 v_A^2} \tag{19}$$

is the approximate ratio of gas to magnetic pressure, while the kinetic ($Re = v_A L_0/(\mu/m_p n_0)$) and magnetic ($Rm = v_A L_0/\eta$) Reynolds numbers express the ratio of convective to dissipative effects in each equation. The Hall parameter

$$\epsilon = \frac{c}{\omega_{pi} L_0} = \sqrt{\frac{m_p c^2}{4\pi e^2 n_0 L_0^2}} \tag{20}$$

expresses the relative importance of the Hall effect. For $\epsilon \to 0$, the induction Eq. (18) reduces to the one for one-fluid magnetohydrodynamics.

Eqs. (17) and (18) are also known as the Hall-MHD (HMHD) equations. The HMHD system has been extensively studied in recent years, both analytically and numerically. For instance, Hall-MHD has been applied to advance our understanding of dynamo mechanisms (Mininni et al., 2003), magnetic reconnection (Mozer et al., 2002; Smith et al., 2004; Morales et al., 2005), accretion (Wardle et al., 303,; Balbus and Terquem, 2001) or the physics of turbulent regimes (Matthaeus et al., 2003; Mininni et al., 2005; Galtier, 2006; Dmitruk and Matthaeus, 2006). Potential limitations in the validity of Hall-MHD from the more comprehensive framework of Vlasov–Maxwell kinetic theory have been recently pointed out by Howes (2009) and also by Schekochihin et al. (2009). In particular, Howes (2009) shows that Hall-MHD is a valid limit of kinetic theory whenever the electron temperature is larger than the ion temperature.

3. Hall-MHD in a strong magnetic field

In the presence of a strong external magnetic field, velocity and magnetic field fluctuations tend to develop fine scale spatial structures across it, while parallel gradients remain comparatively smoother (Shebalin et al., 1983; Oughton et al., 1994; Matthaeus et al., 1998; Oughton et al., 1998). Assuming the external field to point along $\hat{e}_z$, the total (dimensionless) magnetic field is

$$\boldsymbol{B} = \hat{e}_z + \delta\boldsymbol{B}, \quad |\delta\boldsymbol{B}| \approx \alpha \ll 1 \tag{21}$$

where $\alpha = L_\perp/L_\parallel$ represents the typical tilt of magnetic field lines with respect to the $\hat{e}_z$-direction. Therefore, one expects (assuming $L_0 = L_\perp$ to be the typical lengthscale of the problem)

$$\nabla_\perp \approx 1, \quad \partial_z \approx \alpha \ll 1 \tag{22}$$

To ensure that $\boldsymbol{B}$ remains solenoidal, we assume

$$\boldsymbol{B} = \hat{\boldsymbol{e}}_z + \nabla \times (a\hat{\boldsymbol{e}}_z + g\hat{\boldsymbol{e}}_x) \tag{23}$$

The velocity field instead, is decomposed into a solenoidal plus an irrotational flow, i.e.

$$\boldsymbol{U} = \nabla(\varphi\hat{\boldsymbol{e}}_z + f\hat{\boldsymbol{e}}_x) + \nabla\psi \tag{24}$$

where the potentials $a(\boldsymbol{r},t)$, $g(\boldsymbol{r},t)$, $\varphi(\boldsymbol{r},t)$ and $f(\boldsymbol{r},t)$ are all assumed of order $\alpha \ll 1$ and $\psi(\boldsymbol{r},t)$ is of order α^2 (see details in Gómez et al. (2008); and also Bian and Tsiklauri (2009)).

The standard RMHD approximation (Strauss, 1976) only considers the potentials a and φ, which restrict the dynamics to velocity and magnetic field components perpendicular to the external magnetic field. When the Hall effect becomes relevant (i.e. the term proportional to ϵ in Eq. (18)), potentials f, g and ψ should be added to allow nonzero dynamical field components along $\hat{e}_z$ and therefore capture the helical behavior introduced by this effect.

Assuming also $\partial_t \approx 1$ (which corresponds to the fast timescale $L_\perp/v_A$), we obtain, to first order in α in Eqs. (17) and (18)

$$b + \beta p = \text{constant} \tag{25}$$

$$\phi + \varphi - \epsilon(b + \beta_e p_e) = \text{constant} \tag{26}$$

which are Bernoulli conditions constraining the pressures and the electrostatic potential, and correspond to pressure equilibria established over typical timescales of the fast magnetosonic mode. The coefficient β_e in Eq. (26) is $\beta_e = p_{0e}/m_p n_0 v_A^2$.

To follow the evolution of the system on the much slower timescale $L_\parallel/v_A$ (i.e. assuming $\partial_t \approx \alpha \ll 1$), Eqs. (17) and (18) to order α^2 describe the dynamical evolution of the potentials (i.e. a, φ, g and f)

$$\partial_t a = \partial_z(\varphi - \epsilon b) + [\varphi - \epsilon b, a] + \frac{1}{Rm}\nabla^2 a \tag{27}$$

$$\partial_t \omega = \partial_z j + [\varphi, \omega] - [a, j] + \frac{1}{Re}\nabla^2 \omega \tag{28}$$

$$\partial_t b = \beta_* \partial_z (u - \epsilon j) + [\varphi, b] + \beta_* [u - \epsilon j, a] + \beta_* \frac{1}{Rm}\nabla^2 b \tag{29}$$

$$\partial_t u = \partial_z b + [\varphi, u] - [a, b] + \frac{1}{Re}\nabla^2 u \tag{30}$$

where $j = -\nabla_\perp^2 a$ and $\omega = -\nabla_\perp^2 \varphi$ are, respectively, the parallel current and vorticity components, and $[a,b] = \partial_x a \partial_y b - \partial_y a \partial_x b$ indicate the standard Poisson brackets. The parallel component of the dynamical magnetic field is $b = -\partial_y g$, and that of the velocity field is $u = -\partial_y f$. The coefficient β_* is (see also Bian and Tsiklauri (2009))

$$\beta_* = \frac{\gamma\beta}{1+\gamma\beta} \tag{31}$$

where β is the coefficient defined in Eq. (19) and γ is the polytropic index (see Eqs. (9) and (10)). In summary, the set of Eqs. (27)–(30) describe the dynamical evolution of a Hall plasma embedded in a strong external magnetic field.

Just as for three-dimensional Hall-MHD, this set of equations display three ideal invariants: the energy

$$\begin{aligned} E &= \frac{1}{2}\int d^3r\ (|\boldsymbol{U}|^2 + |\boldsymbol{B}|^2) \\ &= \frac{1}{2}\int d^3r\ (|\nabla_\perp\varphi|^2 + |\nabla_\perp a|^2 + u^2 + b^2), \end{aligned} \tag{32}$$

the magnetic helicity

$$H_m = \frac{1}{2}\int d^3r\ (\boldsymbol{A}\cdot\boldsymbol{B}) = \int d^3r\ ab \tag{33}$$

and the hybrid helicity (Turner, 1983; Mahajan and Yoshida, 2000)

$$\begin{aligned} H_h &= \frac{1}{2}\int d^3r\ (\boldsymbol{A}+\epsilon\boldsymbol{U})\cdot(\boldsymbol{B}+\epsilon\boldsymbol{\Omega}) \\ &= \int d^3r\ [ab + \epsilon(a\omega + ub) + \epsilon^2 u\omega)] \end{aligned} \tag{34}$$

where $\boldsymbol{\Omega} = \nabla\times\boldsymbol{U}$ is the vorticity vector field.

4. Application of RHMHD to solar wind turbulence

The relative importance of the Hall effect in the Hall-MHD equations (i.e. Eqs. (17) and (18)) is determined by the coefficient ϵ, which is only present in Eq. (18). From the expression of ϵ in Eq. (20), we find that the Hall effect must become non-negligible in sufficiently low density plasmas. One of the many low-density astrophysical plasmas for which the Hall effect is known to be relevant is the solar wind, and it becomes progressively more important as we move away from the Sun. Also, the solar wind plasma is permeated by an external magnetic field (although the magnetic fluctuations can be a non-negligible fraction of the external field).

To study the role of the Hall effect on the energy power spectrum, we integrate Eqs. (27)–(30) numerically. We assume periodicity for the lateral boundary conditions, and specify the velocity fields at the boundaries $z = 0$ and $z = L$ (for a detailed description, see Dmitruk et al. (2003)). These boundary motions pump energy into the system and drives it into a turbulent regime. We use a pseudo-spectral technique with dealiasing for the perpendicular spatial derivatives and finite differences for the (much smoother) $\hat{e}_z$-derivatives. We start all our simulations with trivial initial conditions (i.e. $a = \varphi = u = b = 0$).

We performed a set of simulations with different values of the Hall parameter (see details in Gómez et al. (2008)). Among the results arising from these simulations, we find that the fraction of kinetic to total energy increases monotonically with the Hall coefficient ϵ.

In the MHD limit ($\epsilon = 0$), the total energy reduces to (Eq. (32))

$$E_{perp} = \frac{1}{2}\int d^3r\ (|\nabla_\perp\varphi|^2 + |\nabla_\perp a|^2) \tag{35}$$

while for the general case ($\epsilon \neq 0$) there is a fraction of the total energy directly associated to the parallel degrees of freedom

$$E_{par} = \frac{1}{2}\int d^3r\ (u^2 + b^2) \tag{36}$$

The fraction E_{par}/E_{tot} is also observed to increase monotonically with ϵ, even though we are not pumping parallel energy from the boundaries. Parallel fluctuations are generated by the perpendicular part of the dynamics (i.e. by a and φ) via terms proportional to ϵ in Eq. (29).

We expect the Hall current to affect the dynamics of spatial patterns whose sizes are of the order of the ion skin depth (i.e. c/w_{pi}) or smaller. According to Eq. (20), this typical size corresponds to a $k_\epsilon = 1/\epsilon$. In Fig. 1 we compare the spectral distributions of energy for $\epsilon = 0.0$ and $\epsilon = 0.1$, once a stationary turbulent regime is reached for each of these simulations. Even though these numerical simulations have only a moderate spatial resolution of $512\times512\times32$, the energy spectra are consistent with the slope predicted by Kolmogorov (i.e. $E_k \propto k^{-5/3}$) at intermediate and large scales (i.e. intermediate and small values of k). We also find that both the total and kinetic energy spec-

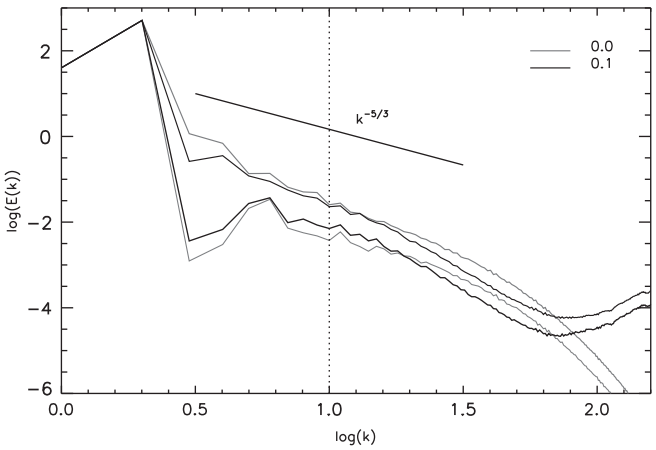

Fig. 1. Energy power spectra for $\epsilon = 0.0$ (thick gray trace) and $\epsilon = 0.1$ (thick black trace) for a $512\times512\times32$ run at $t = 20$. The Kolmogorov slope is displayed for reference, and the vertical dashed line indicates the location of $k_\epsilon = 1/\epsilon$ for $\epsilon = 0.1$. The thin lines show the power spectra for the corresponding kinetic energies.

tra for the simulation corresponding to $\epsilon = 0.1$, strongly depart from the purely MHD run (i.e. $\epsilon = 0.0$) for $k \geqslant k_\epsilon$.

The spectral distribution of energy dissipation is given by $2\eta k^2 E(k)$. Fig. 2 shows energy dissipation spectra for different simulations corresponding to $\epsilon = 0, 1/32, 1/16, 1/8$. We find that the spectral distribution of energy dissipation shifts to larger wavelengths as ϵ rises, which is quantitatively confirmed by the corresponding values of the mean scale defined as

$$k_{mean}^2 = \frac{\int dk k^2 E(k)}{\int dk E(k)} \tag{37}$$

listed in the Table 1.

The scale k_{mean}, also known as the Taylor scale, can be regarded as the average curvature of magnetic fieldlines. Its gradual shift with the Hall effect is consistent with a reduction of the energy transfer rate associated to the direct energy cascade for $k > k_\epsilon$, which in turn leads to smaller total dissipation rates (Gómez et al. (2010), see also Mininni et al. (2007)).

Another important feature of Hall-MHD in its ideal limit (i.e. for $\eta \to 0$) is the self-consistent presence of a component of the electric field parallel to the total magnetic field, which is able to accelerate charged particles (see also Bian and Kontar (2010) and Bian et al. (2010)). Fig. 3 shows the power spectrum of the total electric field, superimposed to the corresponding spectra of kinetic and magnetic energy, for $\epsilon = 0.1$. We can clearly observe an excess of power in the electric field compared to the magnetic field at large wavenumbers (i.e. $k > k_\epsilon$).

The dimensionless version of the electric field (see Eq. (14)) is

$$\boldsymbol{E} = -\left(\boldsymbol{U} - \frac{\epsilon}{n}\nabla \times \boldsymbol{B}\right) \times \boldsymbol{B} - \frac{\epsilon \beta_e}{n}\nabla p_e + \eta \nabla \times \boldsymbol{B} \tag{38}$$

When computing the component of the electric field which is parallel to the magnetic field (i.e. $E_\parallel = \frac{\boldsymbol{E}\cdot\boldsymbol{B}}{|\boldsymbol{B}|^2}$) only two terms contribute, the one proportional to the electron pressure gradient and the one corresponding to electric resistivity. To second order in the expansion coefficient α (see Eq. (21)) and using that $\beta_e p_e = -\frac{\beta_e}{\beta} b$, we obtain

$$E_\parallel = \epsilon \frac{T_e}{T_e + T_p}(\partial_z b + [b, a]) + \eta j \tag{39}$$

In Fig. 4 we show two histograms corresponding to the terms proportional to ϵ (black) and η (gray) in Eq. (39), assuming $T_e \gg T_p$. We can clearly see that the contribution of the Hall effect to $E_\parallel$, which is actually caused by the $\nabla_\parallel p_e$ term in Eq. (38), is markedly larger than the contribution of the plasma resistivity. Note that the electron pressure is cast in terms of the parallel magnetic field component b as a result of Eq. (25).

We need simulations at much higher spatial resolution to make quantitative assessments about power spectra or energy dissipation, but these simulations at moderate resolution show that the behavior at small scales (i.e. $k > k_\epsilon$) is clearly affected by the presence of the Hall term. The RHMHD framework has been numerically tested against the more general compressible Hall-MHD description (Martín et al., 2010). The results show that the degree of agreement between both sets of simulations is very high when the various assumptions for RHMHD are satisfied, thus rendering RHMHD as a valid approximation of Hall-MHD in the presence of strong external magnetic fields.

Table 1
Hall and mean scales.

Run	ϵ	k_{Hall}	k_{mean}
1	0	∞	8.5
2	1/32	32	8.2
3	1/16	16	7.7
4	1/8	8	7.2

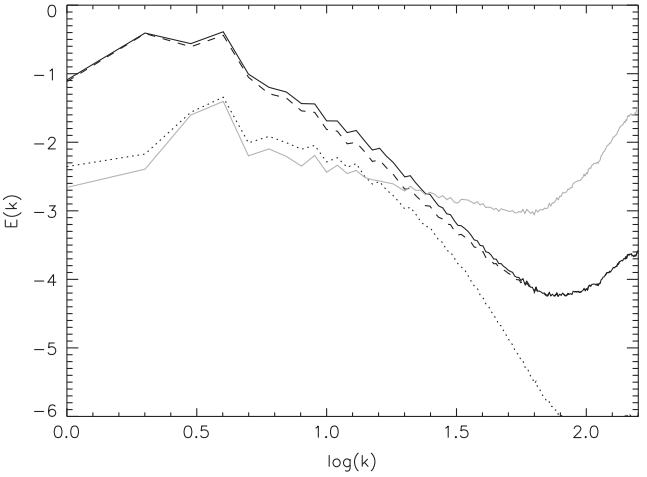

Fig. 3. Energy power spectra for a $512 \times 512 \times 32$ run with $\epsilon = 0.1$ at $t = 20$. Black full trace corresponds to total energy, dotted (dot-dashed) trace to kinetic (magnetic) energy, and the gray full trace shows the power spectrum of the electric field.

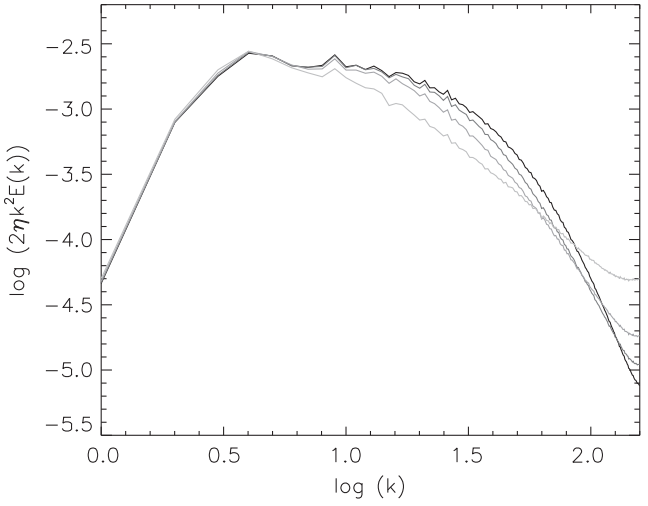

Fig. 2. Spectral distribution of energy dissipation for simulations corresponding to $\epsilon = 0, 1/32, 1/16, 1/8$, displayed in gradually lighter shades of gray.

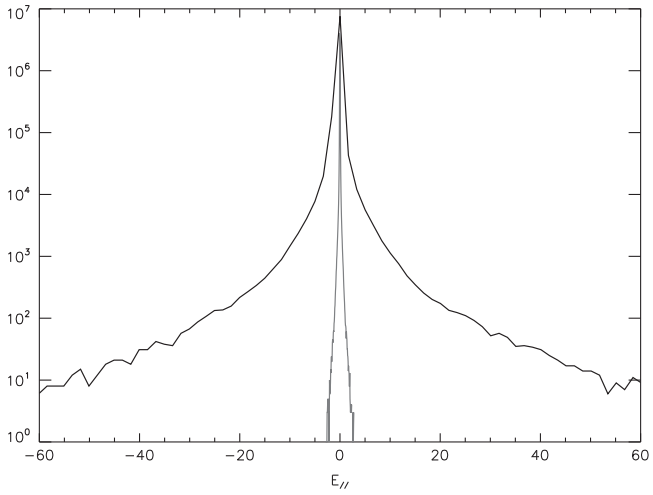

Fig. 4. Histograms of the terms proportional to ϵ (black) and η (gray) for $E_{\parallel}$ (see Eq. (39) for a $512 \times 512 \times 32$ run with $\epsilon = 0.1$ and $t = 20$.

5. Application of RMHD to coronal heating

Another application of the reduced approximation to an astrophysical problem, is the simulation of magnetic loops of the solar corona, to study the heating of the plasma confined in coronal magnetic structures. To model the internal dynamics of coronal loops in solar (or stellar) active regions, we assume these loops to be relatively homogeneous bundles of fieldlines, with their footpoints deeply rooted into the photosphere. Individual fieldlines are moved around by subphotospheric convective motions, which in turn generate magnetic stresses in the coronal portion of the loop. We therefore consider a magnetic loop with length L and cross section $2\pi l_{ph} \times 2\pi l_{ph}$, where l_{ph} is the lengthscale of typical subphotospheric motions. For elongated loops, *i.e.* such that $2\pi l_{ph} \ll L$, we neglect toroidal effects. The main magnetic field $\mathbf{B_0}$ is assumed to be uniform and parallel to the axis of the loop (the z axis) and the perpendicular planes at $z = 0$ and $z = L$ correspond to the photospheric footpoints. For the coronal plasma, the Hall effect is actually negligible, so we simply integrate the RMHD equations (i.e. $\epsilon = 0.000$).

As boundary conditions, we assume $\psi(z = 0) = 0$ and $\psi(z = L) = \Psi(x, y)$ where the stream function $\Psi(x, y)$ describes stationary and incompressible footpoint motions on the photospheric plane (see Dmitruk et al. (2003)). We specify the Fourier components of $\Psi(x, y)$ as $\Psi_{\mathbf{k}} = \Psi_0$ inside the ring $3 < l_{ph}|k| < 4$ on the Fourier plane, and $\Psi_{\mathbf{k}} = 0$ elsewhere, to simulate a stationary and isotropic pattern of photospheric granular motions of diameters between $2\pi l_{ph}/4$ and $2\pi l_{ph}/3$. The strength Ψ_0 is proportional to a typical photospheric velocity $V_{ph} \approx 1$ km s^{-1}. The typical timescale associated to these driving motions, is the eddy turnover time, which is defined as $t_{ph} = l_{ph}/V_{ph} \approx 10^3$ s. We choose a narrowband and non-random forcing to make sure that the broadband energy spectra and the signatures of intermittency that we obtain are exclusively determined by the nonlinear nature of the MHD equations.

In Fig. 5 we show the results obtained from a simulation extending from $t = 0$ to $t = 100\ t_A$, where $t_A = L/v_A$ is the Alfven time of the loop. The upper panel shows the kinetic (E_U, thin trace) and total energy ($E = E_U + E_B$, thick trace). We can see that after about ten Alfven times, the energy reaches a stationary regime, since the work done by footpoint motions statistically (i.e. in time average) reaches an equilibrium with the dissipative processes (electric resistivity and fluid viscosity). In this stationary regime most of the energy is magnetic, while kinetic energy is only about 5% of the total. In the lower panel, we show the dissipation rate (D, thick trace) and the incoming Poynting flux (P, thin trace), showing that their time averages are approximately equal.

The observed stationary equilibrium has been shown to correspond to a turbulent regime (Gómez and Ferro Fontán, 1988, 1992), and therefore the associated energy cascade bridges the gap between the large spatial scales where energy is injected by footpoint motions, to the much smaller scales where it dissipates (see Dmitruk and Gómez (1997)). The dependence of the stationary dissipation rate $< D >=< P >$ ($< \cdots >$: time average) with the physical parameters of the loop is (Dmitruk and Gómez, 1999)

$$\langle D \rangle \propto \frac{\rho l_{ph}^2}{t_A^3} \left(\frac{t_A}{t_{ph}} \right)^{\frac{3}{2}} \tag{40}$$

In Fig. 5 we can clearly observe the spiky nature of these time series, which is the result of the intermittency arising

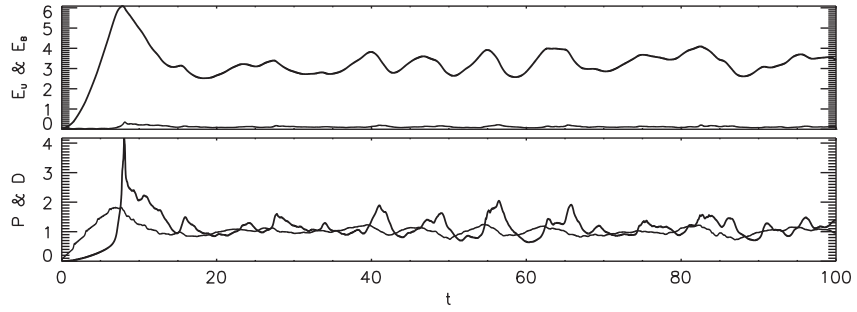

Fig. 5. Energy and dissipation rate time series. **Upper panel**: kinetic energy (thin), and total energy (thick). **Lower panel**: energy dissipation rate (thick) and Poynting flux (thin).

in turbulent regimes. Dmitruk et al. (1998) associated these spikes of energy dissipation with Parker's *nanoflares* (see Parker (1988)) and studied the statistical distribution of these dissipation events. A detailed description of that statistical study is beyond the scope of this presentation, but the main result (see also Gómez and Dmitruk (2008)) is that the number of nanoflares (or spikes) as a function of their energies $N(E)$ follows a power law $N(E) \approx E^{-3/2}$, which is remarkably comparable to the result obtained for larger dissipation events. The statistics of large energy dissipation events such as microflares and flares, has been reported by Aschwanden (2004), gathering a large number of observational studies.

6. Conclusions

In this presentation we reviewed the basic features of two-fluid magnetohydrodynamics as a valid theoretical framework for astrophysical and space plasmas. Even though two-fluid MHD is aimed at theoretically describing the relatively large-scale behavior of plasmas, it does nonetheless retain the effects of the Hall current at scales comparable or smaller than the ion skin-depth. For plasmas permeated by relatively strong external magnetic fields, we introduce the reader to the so-called reduced magnetohydrodynamic approximation, which takes advantage of the much smoother spatial structure of these plasmas along magnetic fieldlines.

We also present new numerical results of the reduced MHD equations which are relevant to the following two astrophysical problems: the turbulent dynamics of the solar wind plasma and the turbulent heating of coronal active regions. In the solar wind plasma, the Hall effect becomes progressively more important as we move away from the Sun. Our RHMHD simulations show that the Hall effect is able to produce measurable changes in the energy power spectrum. In particular, the ratio of kinetic to total energy increases with the Hall coefficient ϵ, as well as the ratio of parallel to total energy, confirming previous results (Gómez et al., 2008) with smaller spatial resolution. Moreover, the energy spectrum departs quite noticeably from the $\epsilon = 0.0$ case.

We have also shown numerical results from RMHD simulations (the Hall effect is not likely to be relevant in the coronal plasma) of the internal dynamics of magnetic loops of the solar corona. These simulations show the development of a magnetically dominated and stationary turbulent regime inside the loop, as a result of the persistent action of convective subphotospheric motions. The mean value of the heating rate arising from these simulations is of the same order of magnitude of the main cooling rates in coronal active regions (Dmitruk and Gómez, 1997), namely, radiative losses and thermal conductivity to the chromosphere. Superimposed to this stationary heating rate, simulations also show the ubiquitous presence of spiky heating events, as a result of the intermittent nature of turbulence. The statistics of these heating events or *nanoflares* (see Dmitruk et al. (1998)), is remarkably similar to the one obtained for the much larger dissipation events, known as *flares* (see Aschwanden (2004)).

Acknowledgments

The authors acknowledge constructive comments of two anonymous referees, which contributed to improve an earlier version of this manuscript. P. Dmitruk and D.O. Gómez are members of the Carrera del Investigador Científico of CONICET. This research was supported by grants PIP 11220090100825 from CONICET and grant UBACyT 20020100100315 from the University of Buenos Aires.

References

Aschwanden, M.J. Physics of the Solar Corona: An Introduction. Springer-Verlag, Berlin, 2004.

Balbus, S.A., Terquem, C. Linear analysis of the Hall effect in protostellar disks. Astrophys. J. 552, 235–247, 2001.

Bian, N.H., Tsiklauri, D. Compressible Hall magnetohydrodynamics in a strong magnetic field. Phys. Plasmas 16, 064503, 2009.

Bian, N.H., Kontar, E.P. A gyrofluid description of alfvenic turbulence and its parallel electric field. Phys. Plasmas 17, 062308, 2010.

Bian, N.H., Kontar, E.P., Brown, J.C. Parallel electric field generation by Alfvén wave turbulence. Astron. Astrophys. 519, A114, 2010.

Dmitruk, P., Matthaeus, W.H. A two-component phenomenology for homogeneous magnetohydrodynamic turbulence. Phys. Plasmas 13, 042306, 2006.

Dmitruk, P., Matthaeus, W.H., Oughton, S. Direct comparisons of compressible magnetohydrodynamics and reduced magnetohydrodynamics turbulence. Phys. Plasmas 12, 112304, 2005.

Dmitruk, P., Gómez, D.O., Matthaeus, W.H. Energy spectrum of turbulent fluctuations in boundary driven reduced MHD. Phys. Plasmas 10, 3584–3591, 2003.

Dmitruk, P., Gómez, D.O. Scaling law for the heating of solar coronal loops. Astrophys. J. 527, L63–L66, 1999.

Dmitruk, P., Gómez, D.O., DeLuca, E. MHD turbulence of coronal active regions and the distribution of nanoflares. Astrophys. J. 505, 974–983, 1998.

Dmitruk, P., Gómez, D.O. Turbulent coronal heating and the distribution of nanoflares. Astrophys. J. 484, L83–L86, 1997.

Galtier, S. Wave turbulence in incompressible Hall magnetohydrodynamics. J. Plasma Phys. 72, 721–769, 2006.

Goldston, R.J., Rutherford, P.H. Introduction to Plasma Physics. IOP Publ., Bristol & Philadelphia, 1995.

Gómez, D.O., Mininni, P.D., Dmitruk, P. Hall-magnetohydrodynamic small-scale dynamos. Phys. Rev. E 82, 036406, 2010.

Gómez, D.O., Mahajan, S.M., Dmitruk, P. Hall magnetohydrodynamics in a strong magnetic field. Phys. Plasmas 15, 102303, 2008.

Gómez, D.O., Dmitruk, P., 2008. Turbulent heating of coronal active regions, in: Erdelyi, R., Mendoza-Briceño, C.A. (Eds.), Proc. IAU Symp. 247: Waves and Oscillations in the Solar Atmosphere, pp. 269–278.

Gómez, D.O., Ferro Fontán, C. Development of MHD turbulence in coronal loops. Astrophys. J. 394, 662–669, 1992.

Gómez, D.O., Ferro Fontán, C. Coronal heating by selective decay of MHD turbulence. Sol. Phys. 116, 33–44, 1988.

Hendrix, D.L., van Hoven, G. Magnetohydrodynamic turbulence and implications for solar coronal heating. Astrophys. J. 467, 887–893, 1996.

Howes, G.G. Limitations of Hall MHD as a model for turbulence in weakly collisional plasmas. Nonlinear Proc. Geophys. 16, 219–232, 2009.

Krall, N.A., Trivelpiece, A.W. Principles of Plasma Physics. McGraw-Hill, New York, pp. 89, 1973.

Longcope, D.W., Sudan, R.N. Evolution and statistics of current sheets in coronal magnetic loops. Astrophys. J. 437, 491–504, 1994.

Mahajan, S.M., Yoshida, Z. A collisionless self-organizing model for the high-confinement (H-mode) boundary layer. Phys. Plasmas 7, 635–640, 2000.

Martín, L.N., Dmitruk, P., Gómez, D.O. Hall effect in a strong magnetic field: direct comparisons of compressible MHD and the reduced Hall-MHD equations. Phys. Plasmas 17, 112304, 2010.

Matthaeus, W.H., Dmitruk, P., Smith, D., Ghosh, S., Oughton, S. Impact of Hall effect on energy decay in magnetohydrodynamic turbulence. Geophys. Res. Lett. 30, 2104, 2003.

Matthaeus, W.H., Oughton, S., Ghosh, S., Hossain, M. Scaling of anisotropy in hydromagnetic turbulence. Phys. Rev. Lett. 81, 2056–2059, 1998.

Milano, L., Dmitruk, P., Mandrini, C.H., Gómez, D.O., Demoulin, P. QSLs in a reduced magnetohydrodynamics model of a coronal loop. Astrophys. J. 521, 889–897, 1999.

Mininni, P.D., Alexakis, A., Pouquet, A. Energy transfer in Hall-MHD turbulence: cascades, backscatter, and dynamo action. J. Plasma Phys. 73, 377, 2007.

Mininni, P.D., Gómez, D.O., Mahajan, S.M. Direct simulations of helical Hall MHD turbulence and dynamo action. Astrophys. J. 619, 1019–1027, 2005.

Mininni, P.D., Gómez, D.O., Mahajan, S.M. Role of the Hall current in MHD dynamos. Astrophys. J. 584, 1120–1126, 2003.

Morales, L.F., Dasso, S., Gómez, D.O. The Hall effect in incompressible magnetic reconnection. J. Geophys. Res. 110, A04204, 2005.

Montgomery, D.C. Major disruptions, inverse cascades, and the Strauss equations. Phys. Scr. T2 (1), 83–88, 1982.

Mozer, F., Bale, S., Phan, T.D. Evidence of diffusion regions at a subsolar magnetopause crossing. Phys. Rev. Lett. 89, 015002, 2002.

Oughton, S., Matthaeus, W.H., Ghosh, S. Scaling of spectral anisotropy with magnetic field strength in decaying magnetohydrodynamic turbulence. Phys. Plasmas 5, 4235–4242, 1998.

Oughton, S., Priest, E.R., Matthaeus, W.H. The influence of a mean magnetic field on three-dimensional magnetohydrodynamic turbulence. J. Fluid Mech. 280, 95–117, 1994.

Parker, E.N. Nanoflares and the solar X-ray corona. Astrophys. J. 330, 474–479, 1988.

Schekochihin, A.A., Cowley, S.C., Dorland, W., Hammett, G.W., Howes, G.G., Quataert, E., Tatsuno, T. Astrophysical gyrokinetics: kinetic and fluid turbulent cascades in magnetized weakly collisional astrophysical plasmas. Astrophys. J. Suppl. 182, 310–377, 2009.

Shebalin, J.V., Matthaeus, W.H., Montgomery, D. Anisotropy in MHD turbulence due to a mean magnetic field. J. Plasma Phys. 29, 525–547, 1983.

Smith, D., Ghosh, S., Dmitruk, P., Matthaeus, W.H. Hall and turbulence effects on magnetic reconnection. Geophys. Res. Lett. 31, 02805, 2004.

Strauss, H. Nonlinear, three-dimensional magnetohydrodynamics of noncircular tokamaks. Phys. Fluids 19, 134–140, 1976.

Turner, L. Hall effects on magnetic relaxation. IEEE Trans. Plasma Sci. PS14, 849–857, 1983.

van Ballegooijen, A.A. Cascade of magnetic energy as a mechanism of coronal heating. Astrophys. J. 311, 1001–1014, 1986.

Wardle, M., Ng, C. The conductivity of dense molecular gas. Mon. Not. R.A.S. 303, 239–246 (1992) 11, 2214 (2004), 303,.